ACS APPLIED MATERIALS & INTERFACES

Research Article

www.acsami.org

Rapid Removal and Separation of Iron(II) and Manganese(II) from Micropolluted Water Using Magnetic Graphene Oxide

Han Yan, Haijiang Li, Xue Tao, Kun Li, Hu Yang,* Aimin Li, Shoujun Xiao, and Rongshi Cheng

State Key Laboratory of Pollution Control and Resource Reuse, School of the Environment, School of Chemistry and Chemical Engineering, Nanjing University, Nanjing 210093, PR China

Supporting Information

ABSTRACT: A novel two-dimensional carbon-based magnetic nanomaterial, magnetic graphene oxide (MGO), was prepared and then used as an efficient adsorbent. MGO showed rapid and complete removal of iron(II) (Fe) and manganese(II) (Mn) from micropolluted water bodies over a wide pH range. After saturated adsorption, MGO could be rapidly separated from water under an external magnetic field. Results of the adsorption equilibrium study indicated that the adsorption of Fe and Mn by MGO took place via monolayer heterogeneous and spontaneous processes resulting from the heterogeneity of the MGO surface as well as from the electrostatic interactions between surface acidic groups of MGO and metal ions. In addition, both the Fe and Mn uptake of MGO was very slightly affected by NaCl, although it decreased with increased humic acid in solutions. In an Fe/Mn binary aqueous system, both metal ions can be efficiently removed at low concentrations, but MGO showed preferential adsorption of Fe in a concentrated aqueous mixture. The adsorption behavior in the binary system was due to different affinities of surface oxygen-containing functional groups on MGO to Fe and Mn. Finally, unlike traditional approaches in recycling and reusing an adsorbent, the Fe- and Mn-loaded MGO can be directly applied as a new adsorbent to achieve the efficient removal of fluoride from aqueous solutions.

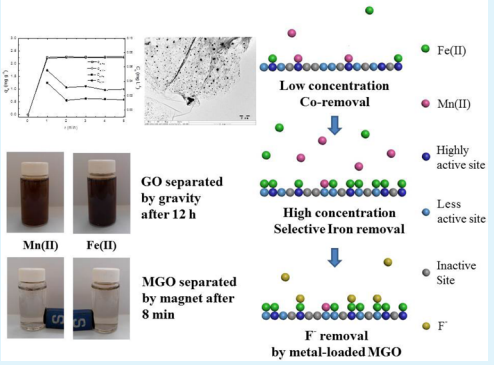

KEYWORDS: *magnetic graphene oxide, removal of iron(II) and manganese(II), selective adsorption, adsorption mechanism*

1. INTRODUCTION

Groundwater containing iron(II) (Fe) and manganese(II) (Mn) is widely distributed in China and coexists with other types of contaminants in different water bodies. The amount of Fe in Chinese groundwater typically is below 5−10 mg L^{-1} and that of Mn ranges from 0.5 to 2.0 mg L^{-1}, respectively.[1] It has been reported that the presence of excessive Fe and Mn in water results in an unpleasant color and odor as well as laundry staining.[2] Their presence also increases health risks, such as cognitive disorder in human beings, especially after long-term intake of water rich in Fe or Mn.[3,4] When Fe- or Mn-rich water is employed in paper and textile production, printing, and dyeing as well as in the chemical and fine leather industries, the quality of the final products is reduced significantly.[2] Therefore, efficient removal of Fe and Mn has always been a major issue in water treatment. The maximum Fe and Mn levels in drinking water in China are 0.3 and 0.1 mg L^{-1}, respectively, (GB5749-2006) which are strictly monitored.[5−7]

Fe and Mn are conventionally removed by aeration and oxidation combined with filtration or sedimentation.[5,6] Although these techniques are commonly used, they are also time-consuming; thus, they are not ideal for rapid purification. Adsorption is capable of removing trace levels of pollutants, including Fe and Mn, and has gained popularity in water treatment applications because of its high efficiency and relatively simple operation.[8] Many kinds of efficient adsorbents have been reported.[9−12] Among these, the application of graphene oxide (GO), a two-dimensional (2D) carbon-based nanomaterial, has attracted significant attention because of its advantages, such as a large surface area, more activated functionalized sites, easy preparation, and good biocompatibility.[9,13−15] These features ensure that GO can facilitate the rapid and efficient removal of pollutants, and numerous studies on the application of GO in water treatment and environmental remediation have been performed in recent years.[16,17] Moreover, the rapid separation of adsorbents after saturated adsorption from water is also significant for recycling both sorbates and adsorbents. However, this may become difficult if the adsorbent has a very small size. Recently, magnetic adsorbents have proven to be easily and rapidly separated from liquid media under an external magnetic field.[18]

In the current work, a novel GO-based magnetic nanomaterial, magnetic graphene oxide (MGO), was prepared after being impregnated with magnetism. We then carried out the adsorptive treatment for the removal of Fe and Mn using MGO as the adsorbent. Fe and Mn contents in synthetic wastewater

Received: April 22, 2014
Accepted: April 30, 2014
Published: April 30, 2014

were controlled at low levels as micropolluted water bodies in order to simulate actual Chinese groundwater sources. To explore the adsorption mechanism, the fundamental adsorption behaviors of MGO, including the effects of the initial solution pH, additives, isothermal adsorption equilibrium, and adsorption kinetics, were investigated. Furthermore, because the two metal ions often coexist in water, a study on the adsorptive removal of both Fe and Mn in a binary aqueous system was also done. Finally, a novel method was carried out to reuse the Fe- and Mn-loaded adsorbents, in which they were directly applied as new adsorbents for the removal of another pollutant. Fluoride (F), a common pollutant found in various water sources, was selected as the target pollutant for secondary adsorption.

2. MATERIALS AND METHODS

2.1. Materials. Graphite was purchased from Tianjin Institute of Chemical Reagents. H_2SO_4, HCl, $KMnO_4$, $NaNO_3$, NaOH, $(NH_4)_2Fe(SO_4)_2{\cdot}6H_2O$, and humic acid (HA) were obtained from Sinopharm Chemical Reagent Co. Ltd. $FeCl_3{\cdot}6H_2O$, ammonia solution, $FeCl_2{\cdot}4H_2O$, $MnCl_2{\cdot}4H_2O$, NaF, and NaCl were purchased from Nanjing Chemical Reagent Co. Ltd. All of the reagents were of analytical grade.

2.2. Preparation of MGO. Prior to MGO preparation, GO was obtained on the basis of Hummers method,[19] for which $KMnO_4$ was used as oxidant. Next, the structure of GO was characterized by Raman spectroscopy, wide-angle X-ray diffraction (XRD), and X-ray photoelectron spectroscopy (XPS), the details of which have been described in our previous work.[20] The resulting Raman and XRD spectra of GO are shown in Supporting Information Figures S1 and S2, respectively. The average aromatic cluster size in GO, based on the intensity ratio of G/D peaks in the Raman spectrum,[21] was 1.32 nm. Meanwhile, the interplanar distance (d) of the oxidized carbon planes according to the Bragg equation was about 0.80 nm from the XRD spectrum, and the oxygen content on the GO surface estimated from the XPS spectrum was approximately 32.81%. Furthermore, the content of various surface oxygen-containing acidic groups of GO (i.e., carboxyl, lactonic, and phenolic groups), as determined by the Boehm titration method, were 2.3, 4.1, and 0.9 mmol g^{-1}, respectively[22] (see Supporting Information Text S1 for details).

The MGO was prepared through in situ coprecipitation of Fe_3O_4 on GO. The experimental details were as follows: 1.0 g of GO was dispersed in water together with 2.53 g of $(NH_4)_2Fe(SO_4)_2{\cdot}6H_2O$ and 1.74 g of $FeCl_3{\cdot}6H_2O$. A few drops of 0.1 mol L^{-1} HCl were added into the solution to inhibit Fe(III) hydrolysis. The mixture was heated at 353 K under N_2 protection. Then, 10 mL of ammonia solution was added, and the mixture was stirred vigorously. The resultant black suspension was constantly stirred at 353 K for 1 h, after which it was filtered and washed. The final product, MGO, was obtained and kept in water for further use. The Fe_3O_4 content in MGO was 59%, as determined from the concentration of dissolved iron ions by an atomic absorption spectrometer once a known amount of MGO was equilibrated in a 0.1 mol L^{-1} HCl aqueous solution. Then, the content of GO component was deduced to be approximately 41%. Aside from the Raman and XRD spectra shown in Supporting Information Figures S1 and S2, MGO underwent vibration magnetometer (VSM), transmission electron microscopy (TEM), and zeta potential characterizations. The VSM spectrum is shown in Supporting Information Figure S3. The characteristic peaks of GO and Fe_3O_4 were both observed in the Raman and the XRD spectra of MGO; moreover, the saturated magnetization of MGO was 20 emu g^{-1}, indicating that MGO was obtained successfully. The detailed operational conditions of all instrumental characterizations are shown in Supporting Information Table S1.

2.3. Fe and Mn Removal in Respective Single-Component Systems. The adsorption behavior of MGO in the removal of Fe and Mn in their respective single-component systems was studied. Fe and Mn aqueous solutions were prepared from $FeCl_2{\cdot}4H_2O$ and $MnCl_2{\cdot}4H_2O$, respectively.

2.3.1. Effect of Initial Solution pH. The effects of the initial solution pH on the removal of Fe and Mn at 298 K were tested. The initial pH ranges were 4.0 to 7.5 for Fe and 4.0 to 10.0 for Mn. The lower and upper pH limits were set to avoid both the dissolution of magnetic Fe_3O_4 particles under acidic conditions and the precipitation of metal hydroxides in alkaline media. Two sets of initial Fe and Mn concentrations were designed: one was 0.04 mmol L^{-1} (2.24 mg L^{-1} for Fe and 2.20 mg L^{-1} for Mn) for the simulation of real Chinese groundwater sources as micropolluted water bodies and the other was relatively high, 1.5 mmol L^{-1} (84.0 mg L^{-1} for Fe and 82.5 mg L^{-1} for Mn), for the comprehensive investigation of the MGO adsorption performance.

About 0.03 g of MGO was dosed and dispersed in 30 mL of a Fe or Mn aqueous solution with different initial pH levels. The mixture was constantly agitated for 4 h to achieve adsorption equilibrium. The final concentrations of Fe and Mn were determined on a Thermo M6 atomic absorption spectrometer. Both flame and furnace methods were adopted, and proper calibration was also performed to ensure the consistency of the different methods. All analyses were peformed in triplicate, and the final metal concentration results are the average of three runs, for which the relative error was lower than 1.0%.

In addition, effects of initial solution pH on the adsorption performance of pure Fe_3O_4 nanoparticles for the removal of Fe and Mn in respective single-component water bodies were also studied under the same conditions as those for MGO for further comparison. The initial concentrations of Fe and Mn were 84.0 and 82.5 mg L^{-1}, respectively.

Equilibrium adsorption capacity (q_e, mg g^{-1}) was calculated from the metal concentration change in the adsorption process using the following equation

$$q_e = \frac{(C_0 - C_e)V}{m} \tag{1}$$

where C_0 and C_e (mg L^{-1}) are the initial and equilibrium Fe or Mn concentrations of the mixture, respectively, V (L) is the total volume of the solution at equilibrium, and m (g) is the dried weight of the adsorbent.

The removal rate (R %) was calculated at the same time according to the following equation

$$R\ (\%) = \frac{C_0 - C_e}{C_0} \times 100\% \tag{2}$$

where C_0 and C_e (mg L^{-1}) are the initial and equilibrium Fe or Mn concentrations of the aqueous mixture, respectively.

2.3.2. Adsorption Equilibrium Study. An adsorption equilibrium experiment was also conducted at 298 K at a pH of approximately 5.5. Then, 0.03 g of MGO was dosed and dispersed in 30 mL of Fe or Mn aqueous solutions with different initial metal concentrations ranging from 0.1 to 90 mg L^{-1}. Each aqueous mixture was agitated for 4 h to achieve adsorption equilibrium. A similar analysis method using the atomic absorption spectrometer, as mentioned above, was employed to detect the initial and final metal concentrations. The metal uptakes were calculated on the basis of eq 1.

2.3.3. Adsorption Kinetics Study. An adsorption kinetics study was also carried out at 298 K and pH 5.5. About 0.2 g of MGO was dispersed in 200 mL of a Fe or Mn solution, and the mixture was then stirred continuously. Two sets of initial concentrations of Fe and Mn, 0.04 and 1.5 mmol L^{-1}, respectively, were designed using the same conditions as described in Section 2.3.1. About 1.0 mL of the mixed solution was taken out at desired time intervals to analyze the current metal concentrations. Meanwhile, the same volume of pure water was added into the bulk solution to keep the volume constant. The metal uptake of MGO at time t_i, $q(t_i)$ (mg g^{-1}) was calculated using the following equation

$$q(t_i) = \frac{(C_0 - C_{t_i})V_o - \sum_2^{i-1} C_{t_{i-1}} V_s}{m} \tag{3}$$

where C_0 and C_{t_i} (mg L^{-1}) are the initial concentration of Fe or Mn and its concentration at time t_i, respectively. V_0 and V_s (L) are the volume of the mixed solution and that of the sample solution taken out each time for concentration analysis, respectively. In this equation, V_s is equal to 1.0 mL. Finally, m (g) represents the mass of the adsorbent.

2.3.4. Effects of Additives. The adsorption performance of MGO in the presence of additives (i.e., NaCl and HA) at 298 K and pH 5.5 was studied. About 0.03 g of MGO was immersed in 30 mL of a metal solution, which contained different amounts of additives. Initial concentrations of Fe and Mn were 2.24 and 2.20 mg L^{-1}, respectively. A similar analysis method using the atomic absorption spectrometer, as mentioned above, was employed to detect the final metal concentrations once adsorption equilibrium was reached.

2.4. Fe and Mn Removal in Binary Systems. The adsorption behavior of MGO for the removal of both metal ions from the Fe/Mn binary aqueous system was carried out at 298 K and pH 5.5. In the adsorption equilibrium experiment, the experimental conditions were similar to those used in the Fe or Mn single-component systems described in Section 2.3.2 except that Fe and Mn coexisted in the solution.

The conditions of the adsorption kinetics experiment were also similar to that in the Fe or Mn single-component system described in Section 2.3.3. The initial concentrations of Fe and Mn in the binary mixture were 2.24 and 2.20 mg L^{-1}, respectively.

2.5. Reuse of MGO. Upon completion of saturated adsorption, the metal-loaded MGOs, denoted MGO-Mn and MGO-Fe, were directly reused as new adsorbents for the removal of F from water at 298 K. The effect of the initial solution pH on F adsorption was investigated. Then, 0.1 g of Fe- or Mn-loaded MGO was immersed in 100 mL of a 1.0 mmol L^{-1} (19 mg L^{-1}) F aqueous solution. The suspension was constantly agitated for 6 h to reach equilibrium. The final residual F concentration was the average of three runs determined using a Mettler Toledo DX-219 F fluorine-selective electrode, for which the relative error was lower than 2.5%. Then, F uptakes were calculated on the basis of eq 1.

3. RESULTS AND DISCUSSION

3.1. Removal of Fe and Mn in Their Respective Single-Component Systems. *3.1.1. Effect of Initial Solution pH.* MGO was prepared using in situ coprecipitation of Fe_3O_4 on GO. The experimental details, including the structural information on MGO, are described in the Materials and Methods. MGO was employed as an adsorbent for the removal of Fe and Mn from the aqueous solutions. pH level is an important factor to ensure a good adsorption performance of ionic-type adsorbents. Thus, in this work, the effect of the initial solution pH on the adsorption of metal ions from single-component micropolluted water bodies was studied, and the results are shown in Figure 1a.

As seen in Figure 1a, most of the removal rates of Fe and Mn under the measured pH range were higher than 95%, and the maximal removal rates were almost 100% at the optimal pH. Furthermore, the residual metal concentrations were mostly compliant with Chinese standards for drinking water quality (GB5749-2006), indicating that MGO was an effective adsorbent for use in the adsorption of Fe and Mn from micropolluted water. The high efficiency of Fe and Mn removal was mainly due to electrostatic interactions among the metal ions and the acidic groups of GO in MGO, because neither the hydrophobic aromatic matrix in the nonoxidation region of GO nor the surface weak positively charged Fe_3O_4[23] can efficiently bind to Fe or Mn in water. On the basis of Supporting Information Figure S4, the pure Fe_3O_4 nanoparticles had really almost no contribution to the adsorption of metal ions from aqueous solutions. Moreover, the highly negative zeta potentials of MGO, as shown in Figure 1b, further confirmed

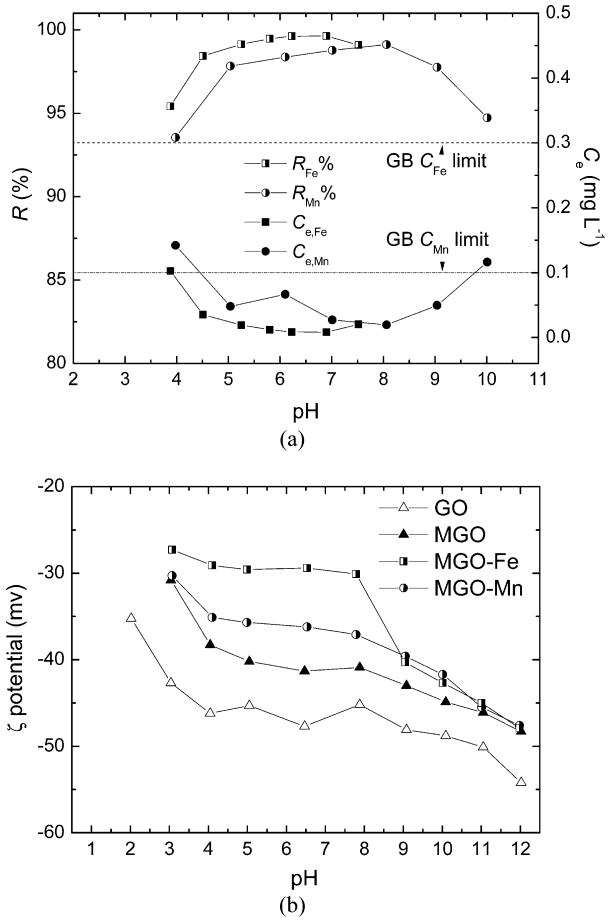

Figure 1. Effects of initial solution pH on the Fe and Mn removal rate and residual concentration by MGO in respective single-component micropolluted water bodies at 298 K. The initial concentrations of Fe and Mn were 2.24 and 2.20 mg L^{-1}, respectively (a); pH dependence of the zeta potentials of MGO, GO, MGO-Mn, and MGO-Fe (b).

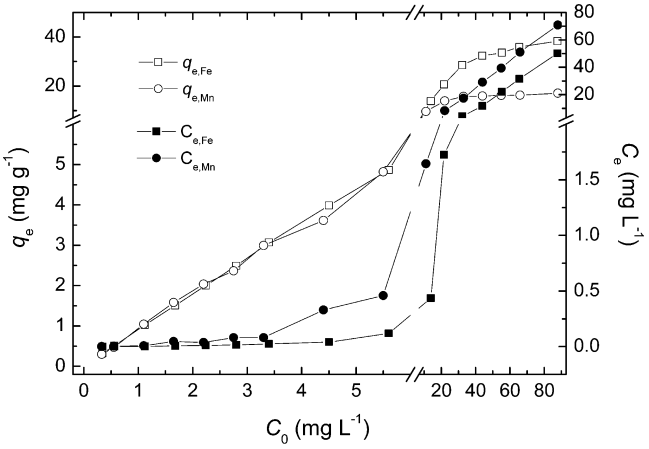

Figure 2. Adsorption isotherms of MGO for the removal of Fe and Mn in their respective single-component water bodies at 298 K and a pH of approximately 5.5.

that many oxygen-containing groups with negative charges as active adsorption sites exist in MGO, thus exhibiting good affinity to cationic species. However, the zeta potentials of MGO were less negative than those of GO over the whole measured pH range, resulting from the fact that only 41% of the GO component was included in the MGO. Furthermore, after

dx.doi.org/10.1021/am502377n | ACS Appl. Mater. Interfaces 2014, 6, 9871−9880

Table 1. Isotherms Parameters for the Adsorption of Metal Ions onto MGO at 298 K and a pH of Approximately 5.5

		Langmuir			Freundlich		
metal ions	$q_{m,exp}$ (mg g^{-1})	q_m (mg g^{-1})	b (L mg^{-1})	r^2	K_f	n	r^2
Fe	43.2	30.3	1.86	0.9725	16.1	2.37	0.9873
Mn	16.5	15.0	1.23	0.9480	6.65	2.72	0.9722

Table 2. Adsorption Capacities and Equilibrium Time of Various Adsorbents for the Removal of Fe and Mn

adsorbents	q_{Fe} (mg g^{-1})	q_{Mn} (mg g^{-1})	equilibrium time (min)	refs
MGO			~1.0[a]	this work
	43.2	16.5	~15[b]	
granular activated carbon	3.6	2.5	unknown	11
apatite	57.1−124.2	18.5−126.0	unknown	12
AC derived from agro-residues	0.8	0.9	15[c]	27
			40[c]	
Albizia procera legume substrate	11	8.6	30	28
natural zeolite	1.1	0.08	60	29
adsorbent coal	15	25	60	30
para-phenol-resin		9.5	100	31
natural zeolitic tuff		8.6[d]	1400[d]	32

[a]The initial concentrations of Fe and Mn were 2.24 and 2.20 mg L^{-1}, respectively. [b]The initial concentrations of Fe and Mn were 84.0 and 82.5 mg L^{-1}, respectively. [c]Equilibrium time for Fe and Mn, respectively. [d]It was measured at 298 K.

loading with Fe and Mn, the zeta potentials of MGO-Fe and MGO-Mn both increased, but they were still negative based on Figure 1b. Interestingly, the zeta potentials increase was approximatively proportional to the metal ion uptake, resulting in higher zeta potentials of MGO-Fe than those of MGO-Mn.

In addition, Figure 1a also shows the wide adsorption window of pH for the removal of both Fe and Mn. Removal rates, however, decreased slightly when pH decreased or increased further. Some of the GO anionic groups were protonized under acidic conditions, resulting in a weakened negative charge and adsorption inhibition, as confirmed by the pH dependence of the zeta potentials of both GO and MGO. By contrast, excessive hydroxide ions competed with GO to bind with metal ions under alkaline conditions.

Furthermore, the effect of initial solution pH on Fe and Mn adsorption from synthetic water with high metal concentrations was also determined in order to give a comprehensive investigation of the adsorption performance of MGO (Supporting Information Figure S5). From Figures S5 and 1a, it was found that there is a similar variation trend of adsorption performance with pH at both low and high metal concentrations.

3.1.2. Adsorption Equilibrium Study. The equilibrium isotherm has a fundamental role in describing the interactive behavior between solutes and adsorbent. Thus, the adsorption isotherms of MGO for the removal of Fe and Mn in their respective single-component systems were measured over a wide metal concentration range (Figure 2). In the beginning, the Fe and Mn uptake increased linearly with the initial metal concentrations. Furthermore, both Fe and Mn were almost completely removed by MGO when the initial concentrations were lower than 3.5 mg L^{-1} based on the residual metal concentrations. This result indicated that the adsorption sites on MGO were sufficient and that the adsorption capacity fully relied on the amount of Fe or Mn transported from the bulk solutions to the adsorbent surfaces at lower initial concentrations. Meanwhile, at higher initial concentrations, the adsorption sites on the MGO surfaces were saturated, and the adsorption of metal ions achieved equilibrium.

The equilibrium data were also subjected to Langmuir and Freundlich isothermal models for further investigation of the adsorption mechanism. The Langmuir and Freundlich models were deduced from different theoretic assumptions as follows:[24,25] the former is based on the assumption of monolayer adsorption on a homogeneous surface,[24] whereas the latter is usually applied in describing heterogeneous systems.[25] The equations are expressed as follows

$$q_e = \frac{q_m b C_e}{1 + b C_e} \tag{4}$$

$$q_e = K C_e^{1/n} \tag{5}$$

where q_e is the amount of Fe or Mn adsorbed at equilibrium (mg g^{-1}), C_e is the concentration of Fe or Mn at equilibrium (mg L^{-1}), q_m is the adsorption capacity when the adsorbent is fully covered (mg g^{-1}), b is the Langmuir adsorption constant (L mg^{-1}), K_f is the Freundlich isotherm constant, and n (dimensionless) is the heterogeneity factor.

The fitting results are listed in Table 1. The correlation coefficients (r^2) of the linear forms for the Langmuir and Freundlich models were both high, with those of the Langmuir model being slightly lower. The result indicated that the Langmuir and Freundlich mechanisms may be both involved in MGO adsorption of Fe and Mn. As mentioned earlier, both Fe and Mn were adsorbed through electrostatic interactions with the acidic groups of GO. Thus, on one hand, the MGO adsorption of metal ions was monolayer and partially followed the Langmuir model. On the other hand, various oxygen-containing groups (i.e., carboxyl, lactonic, and phenolic groups) existed and were distributed on the surface of MGO according to its structural characteristics. The various acidic groups clearly bear different activity and adsorption energy levels,[25] thus resulting in a heterogeneous surface of the adsorbent that followed the Freundlich adsorption mechanism. Summarily, the adsorption of Fe and Mn on MGO was a monolayer heterogeneous process.

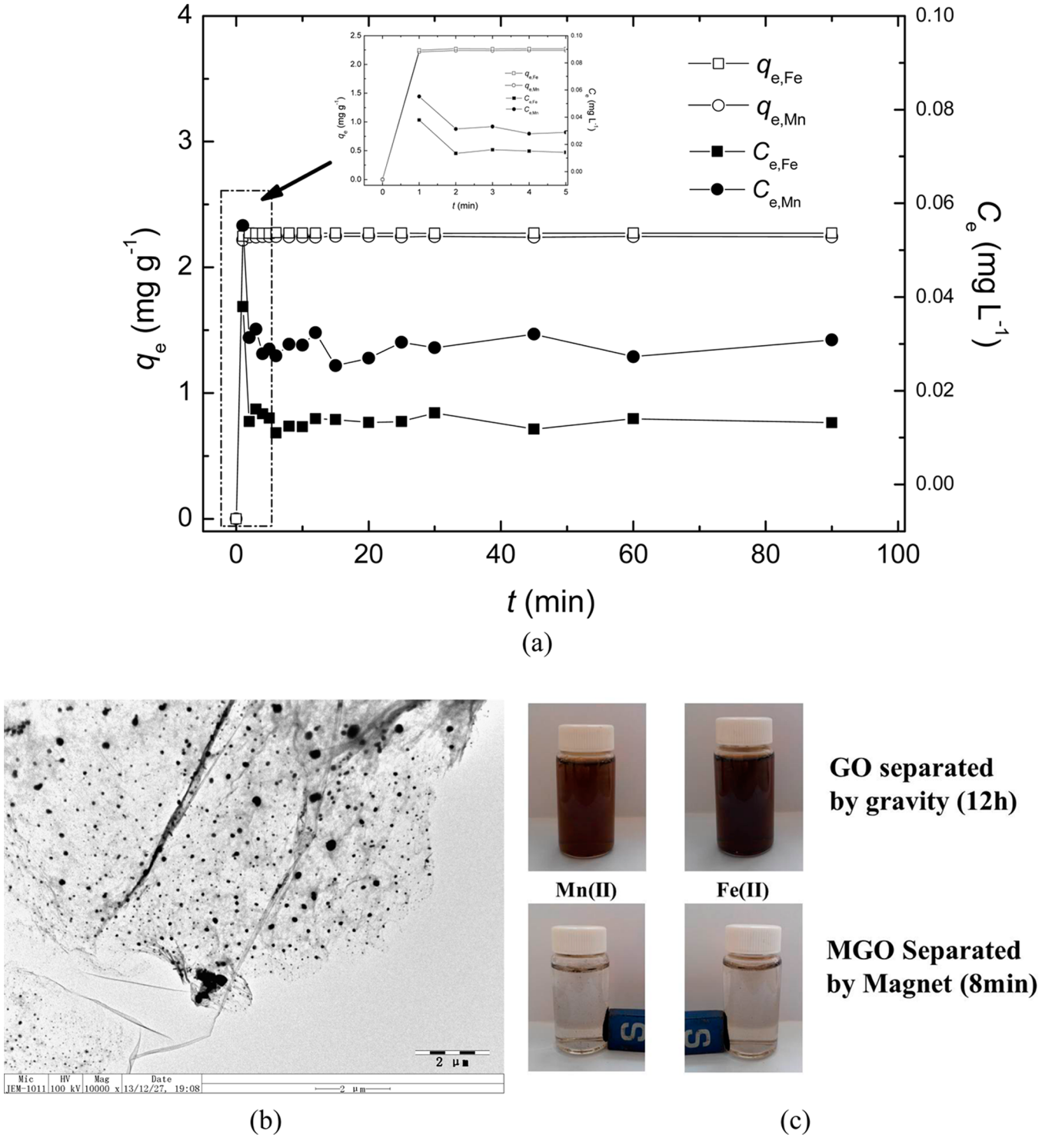

Figure 3. Adsorption kinetics of MGO for removal of Fe and Mn in their respective single-component micropolluted water bodies at 298 K and a pH of approximately 5.5. The initial concentrations of Fe and Mn were 2.24 and 2.20 mg L^{-1}, respectively (a). TEM image of MGO (b). Separation processes of GO by gravity after 12 h and MGO by magnetism (1200 G) after 8.0 min from their aqueous suspensions after adsorption of metal ions (c).

In addition, the thermodynamic parameter of ΔG (kJ mol^{-1}) for the adsorption process can be calculated according to $\Delta G = -RT \ln K_L$. Where R (J mol^{-1} K^{-1}) is the gas constant, T (K) is the temperature, and K_L (L mol^{-1}) is the Langmuir equilibrium constant, which can be obtained by multiplying the constant of b by the molar weight of the metal ions. The ΔG values for the adsorption of Fe and Mn by MGO at 298 K were both negative and approximately −28.6 and −27.5 kJ mol^{-1}, respectively. This indicated that the adsorption processes were spontaneous.

Moreover, the maximum saturated Fe uptake of MGO (about 43.2 mg g^{-1}) was evidently higher than the Mn uptake (about 16.5 mg g^{-1}) (Figure 2). This may be attributed to the fact that Fe is more polarizable than Mn for the relatively inert half-filled electronic arrangement of Mn ($3d^5$) compared with

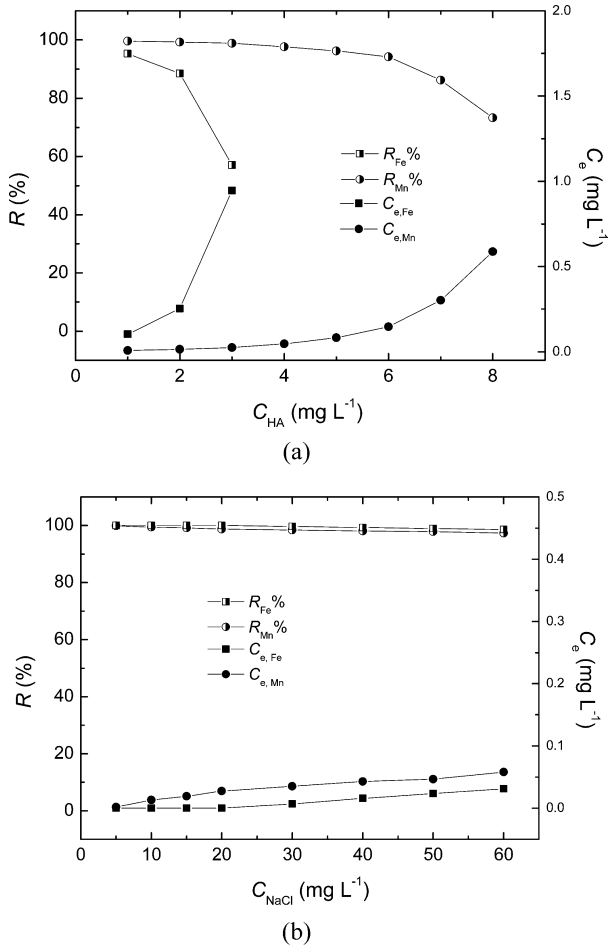

Figure 4. Effect of additives, humic acid (a) and NaCl (b), on Fe and Mn adsorption by MGO in their respective single-component micropolluted water bodies at 298 K and a pH of approximately 5.5. The initial concentrations of Fe and Mn were 2.24 and 2.20 mg L^{-1}, respectively.

that of Fe ($3d^6$),[26] thus resulting in higher Fe uptake and stronger affinity of Fe to those acidic groups. Furthermore, the reaction efficiency of the two metals with the total active sites on MGO can be roughly estimated on the basis of the contents of GO acidic groups in MGO, metal ion uptake, and charge balance. Reaction efficiencies were about 51.5 and 20.0% for Fe and Mn, respectively, thus indicating different activity of the acidic groups and the existence of less active adsorption sites on MGO that bound to Mn with more difficulty than to Fe.

The adsorption capacities of MGO were also compared with those of some other reported adsorbents[11,12,27−32] (Table 2). We found that the Fe and Mn uptake of MGO was higher than that of most adsorbents, indicating that MGO can efficiently remove Fe and Mn from polluted water.

3.1.3. Adsorption Kinetics Study. Adsorption kinetics was also studied to establish the time course of Fe and Mn uptake on MGO in their respective single-component systems. Figure 3a illustrates the variation in the adsorption capacity trends versus contact time for micropolluted water. The adsorption equilibrium for both Fe and Mn was achieved within 1.0 min, which was very rapid compared with aeration and oxidation treatment that usually takes hours.[33] Even for synthetic water with high metal concentrations, adsorption equilibrium was reached in 15 min (Supporting Information Figure S6). Furthermore, in comparison with other reported adsorbents[11,12,27−32] (Table 2), MGO had a much shorter equilibrium time during the adsorption of both Fe and Mn, indicating a higher removal efficiency in terms of both adsorption capacity and speed. The rapid adsorption may be ascribed to two facts: stronger affinity of metal ions to the acidic groups of GO in MGO and good dispersibility of the few-layered MGO sheets. The latter has been confirmed by direct observation under TEM (Figure 3b), resulting in larger surface areas and more activated functionalized sites that are also beneficial to the rapid adsorption of pollutants.

To discuss the adsorption mechanisms further, pseudo-first and pseudo-second order kinetic models[34,35] were applied to the experimental data. The nonlinear forms of the aforementioned kinetics models are presented as eqs 6 and 7, respectively

$$q_t = q_e - q_e e^{-k_1 t} \tag{6}$$

$$q_t = q_e - \frac{q_e}{q_e k_2 t + 1} \tag{7}$$

where q_e and q_t are the amount of Fe or Mn adsorbed onto adsorbents (mg g^{-1}) at equilibrium and at time t (min), respectively. k_1 (min^{-1}) and k_2 (g mg^{-1} min^{-1}) are the rate constants of pseudo-first and pseudo-second order models, respectively.

The simulation results are listed in Supporting Information Table S2. The r^2 of both kinetic models for Fe and Mn were all very high (>0.99) in the two sets of water systems with low and high initial metal concentrations. These results indicated that there were various binding types with different affinity strengths between solutes and adsorbent, which resulted from various activities of different acidic groups on the GO surface. The results of the adsorption kinetics are fully consistent with those of the isothermal adsorption equilibrium discussed earlier.

Rapid separation of adsorbents after saturated adsorption is also very significant. MGO, after evenly complexing with nanomagnets (Figure 3b), exhibited much faster separation in less than 8.0 min (Figure 3c), whereas its precursor GO without magnetism hardly settled down even after 12 h. This suggests the great application potential of MGO for fast removal and separation of Fe and Mn from water bodies.

3.1.4. Effects of Additives. Furthermore, because there are many coexisting solutes in real water, the effects of two common additives, HA (organic matter) and NaCl (inorganic matter), on the adsorption of Fe and Mn were studied in their respective single-component micropolluted water bodies (Figure 4). HA showed an inhibition effect on the adsorption of both Fe and Mn, but the inhibition effect on Fe was more notable (Figure 4a). This may be due to the stronger chelating ability of Fe to HA with its abundant active functional groups.[36] However, when the concentration of HA was below 2.0 mg L^{-1}, the residual concentrations of Fe and Mn were still lower than the upper limits of GB5749-2006.

Compared with organic matter, NaCl showed almost no impact on the adsorption of the two metal ions in the experimental concentration range (Figure 4b). This result indicated that MGO bears salt tolerance in the removal of Fe and Mn from micropolluted water, which can be ascribed to the stronger interaction of Fe and Mn with MGO that cannot be exchanged by Na^+ easily.

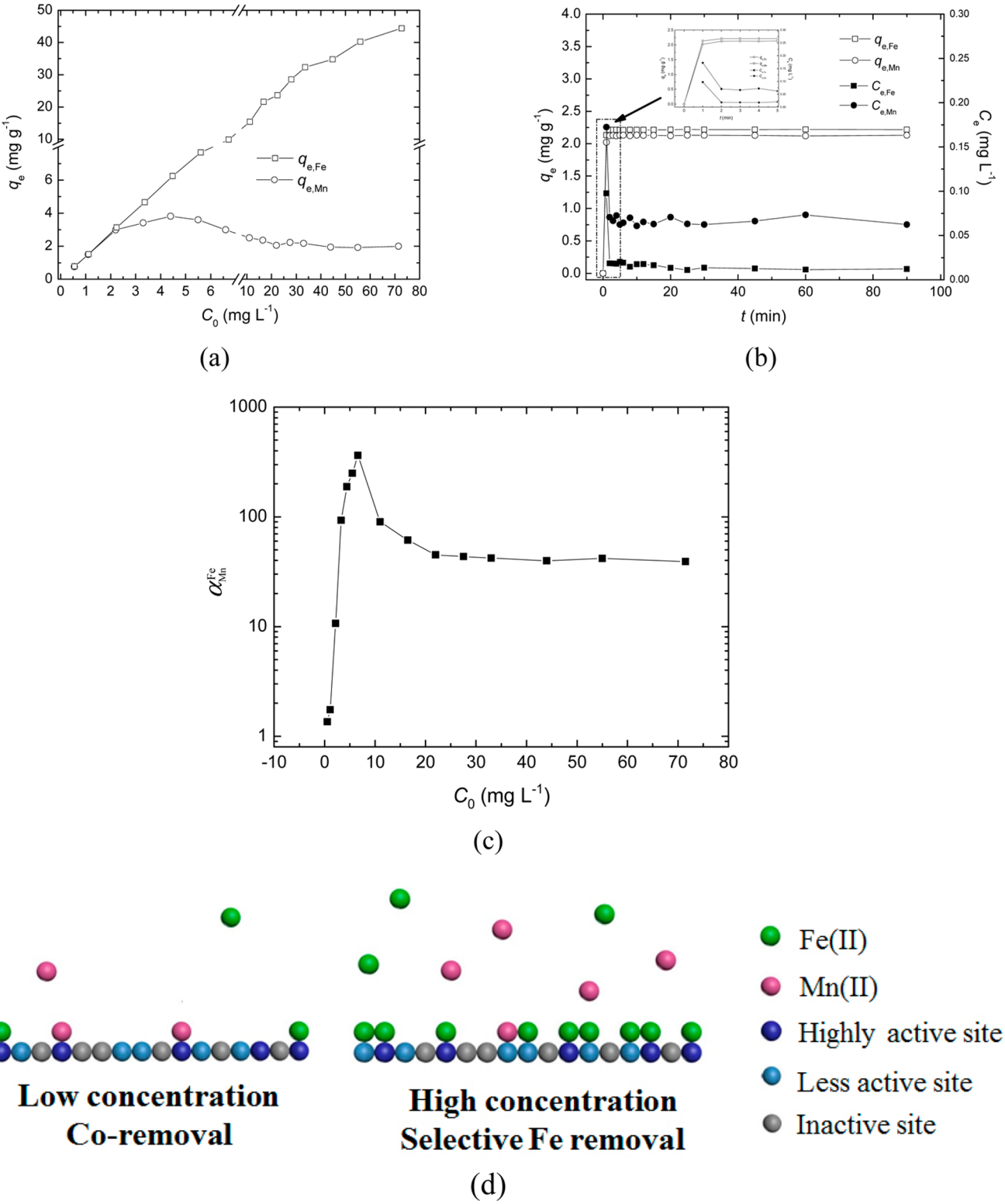

Figure 5. Adsorption behavior of MGO in an Fe/Mn binary water body at 298 K and a pH of approximately 5.5. Adsorption isotherms (a), adsorption kinetics, and the initial concentrations of Fe and Mn were 2.24 and 2.20 mg L^{-1}, respectively (b). Adsorption selectivity (c). Available selective adsorption processes (d).

3.2. Fe and Mn Removal in Binary Systems. It is meaningful to investigate the removal of Fe and Mn under coexisting conditions given that the two ions frequently coexist in water bodies. The adsorption isotherms of MGO for the removal of Fe and Mn in their binary systems are shown in Figure 5a. Compared with their isotherms in their respective single-component systems (Figure 2), the variation trend of Fe was quite similar, but that of Mn was distinctly different. From Figure 5a, Mn and Fe uptake both increased linearly with initial metal concentrations under coexisting conditions. Later, the growth trend of Mn uptake slowed, unlike Fe, and decreased after reaching a maximum (4.5 mg L^{-1}) as the initial metal

dx.doi.org/10.1021/am502377n | ACS Appl. Mater. Interfaces 2014, 6, 9871−9880

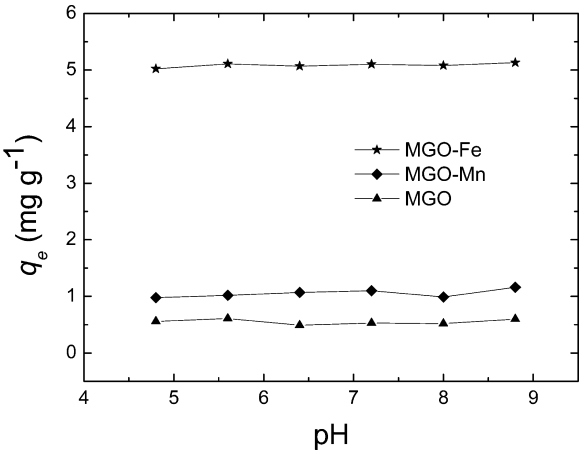

Figure 6. pH dependence of the adsorption capacities of two metal-loaded MGOs and pure MGO for the removal of F at 298 K. The initial concentration of F was 19.0 mg L^{-1}.

concentrations further increased. Moreover, the adsorption rates of both Fe and Mn were still efficient in micropolluted coexisting water, as confirmed by adsorption kinetics experiment (Figure 5b) wherein both metal ions were almost completely removed by MGO from the Fe/Mn binary micropolluted water body based on the residual metal concentrations. In addition, MGO also exhibited very fast removal of Fe and Mn (i.e., only 1.0 min) under coexisting conditions.

However, as the concentrations of Fe and Mn went up, adsorption of Fe was preferred, but that of Mn was inhibited. A selectivity coefficient, α, was introduced for a quantitative description in order to study the adsorption selectivity of MGO toward Fe further. Here, α can be calculated on the basis of the following equation

$$\alpha_{Mn}^{Fe} = \frac{q_{e,Fe}C_{e,Mn}}{C_{e,Fe}q_{e,Mn}} \quad (8)$$

where α_{Mn}^{Fe} is the selectivity factor of Fe over Mn, $q_{e,Fe}$ and $q_{e,Mn}$ are the equilibrium adsorption capacities, and $C_{e,Fe}$ and $C_{e,Mn}$ are the equilibrium concentrations of Fe and Mn, respectively.

On the basis of Figure 5a, α_{Mn}^{Fe} was plotted against the initial metal concentrations listed in Figure 5c, which illustrated the strong selectivity of MGO for Fe because most of the α_{Mn}^{Fe} values were much higher than 1.0. As mentioned earlier, there are various acidic groups (i.e. carboxyl, lactonic, and phenolic groups) on MGO, each with their own adsorption activity. However, the binding constants of Fe with most of the acids were higher than those of Mn,[26] which resulted in a stronger binding affinity of Fe to the active adsorption sites and a higher selectivity of MGO for Fe. The detailed selective adsorption process in the Fe/Mn binary system is described in Figure 5d. In micropolluted water, highly active adsorption sites are sufficient for the efficient removal of Fe and Mn together. When the metal concentrations increased, Fe preferentially occupied the highly active adsorption sites, and some amounts of Mn were expelled and replaced. Moreover, because Mn had a much lower affinity to the residual less active sites on MGO, it was difficult to bind effectively, thus leading to a decrease in Mn uptake and eventual maintenance at a very low level.

3.3. Reuse of MGO. Reusing adsorbents is very important in practical applications. The traditional reuse method involves the recovery of adsorbents by desorption using large amounts of eluent. This is an efficient process, although it can also lead to secondary pollution. Given that the surface structure of MGO after saturated adsorption is distinctly changed but remains stable enough under certain conditions, the Fe- and Mn-loaded adsorbents can be directly applied as new adsorbents for the removal of another pollutant. We attempted to adsorb F, a common pollutant in various water sources, onto metal-loaded MGOs. The results detailed in Figure 6 show that MGO had almost no effect on F removal, whereas the F uptake of MGOs after loading metal ions increased. This indicates that the loaded Fe and Mn play key roles in the adsorption of F from aqueous solutions. Furthermore, MGO-Fe and MGO-Mn both exhibited pH independence for the removal of F over the experimental pH range. This finding may be ascribed to F having a stronger affinity to active adsorption sites (i.e., Fe and Mn on MGO), which can exclude other coexisting ions. Considering the negative zeta potentials of MGO-Mn and MGO-Fe, as shown in Figure 1b, the strong affinity between active adsorption sites and F may be a coordination effect. In addition, the F uptake of MGO-Fe and MGO-Mn was approximately 5.0 and 1.0 mg g^{-1}, respectively. These values are quite comparable with those of previously reported adsorbents,[37−40] suggesting that metal-loaded MGOs are qualified as adsorbents for F removal. Moreover, the higher F uptake of MGO-Fe than that of MGO-Mn may be ascribed to the higher amount of Fe on MGO.

4. CONCLUSIONS

This study highlights the applicability of MGO, a novel 2D carbon-based magnetic nanomaterial, in the removal of Fe and Mn from water. MGO was capable of the rapid removal and separation of both metal ions from micropolluted water bodies over a wide pH range because of the embedded Fe_3O_4 nanoparticles. Furthermore, the residual concentrations of Fe and Mn were fully compliant with Chinese standards for drinking water quality (GB5749-2006). The higher removal efficiencies of MGO in terms of both adsorption capacity and speed were due to a stronger affinity of the metal ions for the oxygen-containing groups of GO. Furthermore, the adsorption of Fe and Mn took place via monolayer heterogeneous and spontaneous processes for the heterogeneous MGO surface containing various acidic groups. In addition, the Fe and Mn uptake of MGO was unaffected by NaCl, but it decreased greatly in the presence of HA, resulting from the higher chelating effects of metal ions with organic matter. In the Fe/Mn binary system, both metal ions can be efficiently removed at low metal concentrations if there are sufficient active adsorption sites. However, at high metal concentrations, Fe was selectively removed, but the adsorption of Mn was fully inhibited. The higher selectivity of MGO for Fe was due to the greater affinity of Fe to the active adsorption sites. Finally, metal-loaded MGOs can be applied as new adsorbents for the direct removal of F. This effective approach provides a zero-cost technique for the reuse of adsorbents. Therefore, the 2D magnetic nanomaterial is expected to be a highly efficient adsorbent for use in future water treatment applications.

■ ASSOCIATED CONTENT

Supporting Information

Details of the Boehm titration of GO; details of the structural characterizations of the samples; nonlinear simulation results of the kinetics data of MGO based on pseudo-first and pseudo-

second order models; Raman spectra of graphite, GO, and MGO; XRD spectra of graphite, GO, and MGO; VSM spectrum of MGO; effect of initial solution pH on the Fe and Mn uptake of pure Fe_3O_4 nanoparticles and MGO; and adsorption kinetics of MGO for the removal of Fe and Mn single-component water bodies. This material is available free of charge via the Internet at http://pubs.acs.org.

AUTHOR INFORMATION

Corresponding Author

*E-mail: yanghu@nju.edu.cn; Tel/Fax: 86-25-89680377.

Funding

This work was supported by the Natural Science Foundation of China (grant nos. 51378250 and 51073077) and by the Open Fund from State Key Laboratory of Pollution Control and Resource Reuse of Nanjing University (grant no. PCRRF11004).

Notes

The authors declare no competing financial interest.

REFERENCES

(1) Zhang, L. S. *The Advanced Water Treatment and Reuse Technology*; Chemical Industry Press: Beijing, 2009.

(2) Ning, R. Y. Colloidal Iron and Manganese in Water Affecting RO Operation. *Desalin. Water Treat.* **2009**, *12*, 162−168.

(3) Dahshan, H.; Abd-Elall, A. M. M.; Megahed, A. M. Trace Metal Levels in Water, Fish, and Sediment from River Nile, Egypt: Potential Health Risks Assessment. *J. Toxicol. Environ. Health* **2013**, *76*, 1183−1187.

(4) Tang, Q.; Liu, G.; Zhou, C.; Zhang, H.; Sun, R. Distribution of Environmentally Sensitive Elements in Residential Soils Near a Coal-Fired Power Plant: Potential Risks to Ecology and Children's Health. *Chemosphere* **2013**, *93*, 2473−2479.

(5) Korchef, A.; Kerkeni, I.; Amor, M. B.; Galland, S.; Persin, F. Iron Removal from Aqueous Solution by Oxidation, Precipitation and Ultrafiltration. *Desalin. Water Treat.* **2009**, *9*, 1−8.

(6) Qin, S. Y.; Ma, F.; Huang, P.; Yang, J. X. Fe(II) and Mn(II) Removal from Drilled Well Water: A Case Study from a Biological Treatment Unit in Harbin. *Desalination* **2009**, *245*, 183−193.

(7) Yuce, G.; Alptekin, C. In situ and Laboratory Treatment Tests for Lowering of Excess Manganese and Iron in Drinking Water Sourced from River−Groundwater Interaction. *Environ. Earth Sci.* **2013**, *70*, 2827−2837.

(8) Yan, H.; Yang, L.; Yang, Z.; Yang, H.; Li, A.; Cheng, R. Preparation of Chitosan/Poly(acrylic acid) Magnetic Composite Microspheres and Applications in the Removal of Copper(II) Ions from Aqueous Solutions. *J. Hazard. Mater.* **2012**, *229*, 371−380.

(9) Sun, Y.; Wang, Q.; Chen, C.; Tan, X.; Wang, X. Interaction between Eu(III) and Graphene Oxide Nanosheets Investigated by Batch and Extended X-ray Absorption Fine Structure Spectroscopy and by Modeling Techniques. *Environ. Sci. Technol.* **2012**, *46*, 6020−6027.

(10) Donia, A. M.; Atia, A. A.; Elwakeel, K. Z. Selective Separation of Mercury(II) Using Magnetic Chitosan Resin Modified with Schiff's Base Derived from Thiourea and Glutaraldehyde. *J. Hazard. Mater.* **2008**, *151*, 372−379.

(11) Bin Jusoh, A.; Cheng, W. H.; Low, W. M.; Nora'aini, A.; Megat Mohd Noor, M. J. Study on the Removal of Iron and Manganese in Groundwater by Granular Activated Carbon. *Desalination* **2005**, *182*, 347−353.

(12) Oliva, J.; De Pablo, J.; Cortina, J.-L.; Cama, J.; Ayora, C. The Use of Apatite II To Remove Divalent Metal Ions Zinc(II), Lead(II), Manganese(II) and Iron(II) from Water in Passive Treatment Systems: Column Experiments. *J. Hazard. Mater.* **2010**, *184*, 364−374.

(13) Chen, D.; Feng, H.; Li, J. Graphene Oxide: Preparation, Functionalization, and Electrochemical Applications. *Chem. Rev.* **2012**, *112*, 6027−6053.

(14) Compton, O. C.; Nguyen, S. T. Graphene Oxide, Highly Reduced Graphene Oxide, and Graphene: Versatile Building Blocks for Carbon-Based Materials. *Small* **2010**, *6*, 711−723.

(15) Wang, J.; Tsuzuki, T.; Tang, B.; Hou, X.; Sun, L.; Wang, X. Reduced Graphene Oxide/Zno Composite: Reusable Adsorbent for Pollutant Management. *ACS Appl. Mater. Interfaces* **2012**, *4*, 3084−3090.

(16) Upadhyay, R. K.; Soin, N.; Roy, S. S. Role of Graphene/Metal Oxide Composites as Photocatalysts, Adsorbents and Disinfectants in Water Treatment: A Review. *RSC Adv.* **2014**, *4*, 3823−3851.

(17) Chowdhury, R.; Balasubramanian, R. Recent Advances in the Use of Graphene-Family Nanoadsorbents for Removal of Toxic Pollutants from Wastewater. *Adv. Colloid Interface Sci.* **2014**, *204*, 35−56.

(18) Rocher, V.; Siaugue, J. M.; Cabuil, V.; Bee, A. Removal of Organic Dyes by Magnetic Alginate Beads. *Water Res.* **2008**, *42*, 1290−1298.

(19) Hummers, W. S. J.; Offeman, R. E. Preparation of Graphitic Oxide. *J. Am. Chem. Soc.* **1958**, *80*, 1339.

(20) Yan, H.; Tao, X.; Yang, Z.; Li, K.; Yang, H.; Li, A.; Cheng, R. Effects of the Oxidation Degree of Graphene Oxide on the Adsorption of Methylene Blue. *J. Hazard. Mater.* **2014**, *268*, 191−198.

(21) Tuinstra, F.; Koening, J.L. Raman Spectrum of Graphite. *J. Chem. Phys.* **1970**, *53*, 1126−1130.

(22) Boehm, H. P. Some Aspects of the Surface Chemistry of Carbon Blacks and Other Carbons. *Carbon* **1994**, *32*, 759−769.

(23) Ahmed, S. M. Studies of the Dissociation of Oxide Surfaces at the Liquid−Solid Interface. *Can. J. Chem.* **1966**, *44*, 1663−1670.

(24) Langmuir, I. The Adsorption of Gases on Plane Surfaces of Glass, Mica and Platinum. *J. Am. Chem. Soc.* **1918**, *40*, 1361−1402.

(25) Freundlich, H. M. F. Uber Die Adsorption in Lasungen. *Z. Phys. Chem.* **1906**, *57*, 385−470.

(26) Dean, J. A. *Lange's Handbook Of Chemistry*; Mcgraw-Hill: New York, 1999.

(27) Akl, M. A.; Yousef, A. M.; Abd El Nasser, S. Removal of Iron and Manganese in Water Samples Using Activated Carbon Derived from Local Agro-Residues. *J. Chem. Eng. Proc. Technol.* **2013**, *4*, 1−10.

(28) Kose, T. D.; Gharde, B. D.; Gholse, S. B. Studies on *Albizia procera* Legumes for Effective Removal of Fe(II) and Mn(II) from Aqueous Solution. *J. Chem. Pharm. Res.* **2012**, *4*, 2021−2028.

(29) Shavandi, M. A.; Haddadian, Z.; Ismail, M. H. S.; Abdullah, N.; Abidin, Z. Z. Removal of Fe(III), Mn(II) and Zn(II) from Palm Oil Mill Effluent (POME) by Natural Zeolite. *J. Taiwan Inst. Chem. Eng.* **2012**, *43*, 750−759.

(30) Vistuba, J. P.; Nagel-Hassemer, M. E.; Lapolli, F. R.; Lobo Recio, M. Á. Simultaneous Adsorption of Iron and Manganese from Aqueous Solutions Employing an Adsorbent Coal. *Environ. Technol.* **2013**, *34*, 275−282.

(31) Kamel, N. H. M.; Sayyah, E. M.; Abdel-Aal, A. A. Removal of Lead, Cobalt and Manganese from Aqueous Solutions Using a New Modified Synthetic Ion Exchanger. *Arch. Appl. Sci. Res.* **2011**, *3*, 448−464.

(32) Rajic, N.; Stojakovic, D.; Jevtic, S.; Zabukovec Logar, N.; Kovac, J.; Kaucic, V. Removal of Aqueous Manganese Using the Natural Zeolitic Tuff from the Vranjska Banja Deposit in Serbia. *J. Hazard Mater.* **2009**, *172*, 1450−1457.

(33) Serikov, L. V.; Tropina, E. A.; Shiyan, L. N.; Frimmel, F. H.; Metreveli, G.; Delay, M. Iron Oxidation in Different Types of Groundwater of Western Siberia. *J. Soils Sediments* **2009**, *9*, 103−110.

(34) Lagergren, S. About the Theory of So-Called Sorption of Soluble Substances. *K. Sven. Vetenskapsakad. Handl.* **1898**, *24*, 1−39.

(35) Ho, Y. S.; Mckay, G. Sorption of Dye from Aqueous Solution by Peat. *Chem. Eng. J.* **1998**, *70*, 115−124.

(36) Batchelli, S.; Muller, F. L. L.; Chang, K.-C.; Lee, C.-L. Evidence for Strong but Dynamic Iron-Humic Colloidal Associations in Humic-Rich Coastal Waters. *Environ. Sci. Technol.* **2010**, *44*, 8485−8490.

(37) Kemer, B.; Ozdes, D.; Gundogdu, A.; Bulut, V. N.; Duran, C.; Soylak, M. Removal of Fluoride Ions from Aqueous Solution by Waste Mud. *J. Hazard. Mater.* **2009**, *168*, 888−894.
(38) Sivasankar, V.; Ramachandramoorthy, T.; Chandramohan, A. Fluoride Removal from Water Using Activated and MnO_2-Coated Tamarind Fruit (*Tamarindus indica*) Shell: Batch and Column Studies. *J. Hazard. Mater.* **2010**, *177*, 719−729.
(39) Ghorai, S.; Pant, K. K. Investigations on the Column Performance of Fluoride Adsorption by Activated Alumina in a Fixed-Bed. *Chem. Eng. J.* **2004**, *98*, 165−173.
(40) Alagumuthu, G.; Rajan, M. Equilibrium and Kinetics of Adsorption of Fluoride onto Zirconium Impregnated Cashew Nut Shell Carbon. *Chem. Eng. J.* **2010**, *158*, 451−457.